Mon. Not. R. astr. Soc. (1988) **235,** 315–341

Multiphase cooling flows; a Lagrangian approach

Peter Thomas *Canadian Institute for Theoretical Astrophysics, 60 St George Street, Toronto, Ontario M5S 1A1, Canada*

Accepted 1988 March 23. Received 1988 February 16

Summary. The intracluster medium in clusters of galaxies which contain cooling flows is multiphase with a range of densities on small scales. A simple, source-free Lagrangian model has been developed to study the development of density distributions in the cooling gas. Initially narrow distributions tend towards a universal form as they cool which gives mass deposition profiles in agreement with the observations. Time-dependent models of collapsing inhomogeneous gas clouds suggest that cooling flows play little part in the formation of low-mass galaxies (up to a few times $10^{12} M_{\odot}$) although infall at later stages can have an effect on the structure of the core. They can play an important role, however, in the formation of higher mass systems. The balance of cooling and inflow in a cooling flow can deposit matter in an extended r^{-2} profile resembling that of a massive halo.

1 Introduction

1.1 COOLING FLOWS

Clusters of galaxies contain large amounts of hot, X-ray-emitting gas with temperatures in the range 2–10 keV and a metallicity of ~0.4 solar; see Sarazin (1986) for a review. In about half the observed clusters the radiative cooling time in the core is very much less than a Hubble time and so, in the absence of any heating, the gas will cool to low temperatures. Surrounding gas moves in to maintain pressure support in the centre thereby inducing a large-scale motion which is called a 'cooling flow'. These flows are always associated with a central dominant galaxy (often, but not always a cD galaxy; I will use the abbreviation cd). The mass flow rate can be as high as several hundred solar masses per year. A similar process occurs in normal elliptical galaxies, though on a much smaller scale with mass inflow rates ranging from a few hundredths to a few solar masses per year.

Until recently most analyses of cooling flows have taken the intracluster medium (ICM) or interstellar medium to be homogeneous on scales very much less than the size of the system. In other words it has been assumed that the gas can be adequately described by a slowly varying, characteristic density and temperature which obey the usual hydrodynamical equations. Spatially

resolved X-ray surface brightnesses are available from the Imaging Proportional Counter (IPC) of the *Einstein Observatory*. In general the data, assumed spherically symmetric, are binned in circular annuli about the peak of emission and are then deprojected, using a procedure first described by Fabian *et al.* (1981), to give the count emissivity profile (luminosity density versus radius). The density and temperature profiles of the gas can then be obtained once the gravitational potential is specified. The most extensive survey of over 100 clusters is that of Arnaud (1985, 1988); only a few early-type galaxies have useful data since they are fainter (Thomas *et al.* 1986). Profiles of mass deposition within radius r, $\dot{M}(<r)$, which equal the mass inflow rates, $\dot{M}(r)$, in a steady state, can then be estimated using the energy equation. It is found that $\dot{M}$ increases with r, implying that matter is deposited throughout the system. The most recent studies for clusters (Arnaud 1985; Arnaud & Fabian 1988) and for galaxies (Thomas *et al.* 1986) use an energy equation which allows for this varying $\dot{M}$ and confirm earlier results.

Studies of the X-ray emission from the Perseus (Fabian *et al.* 1981) and Virgo clusters (Stewart *et al.* 1984) give $\dot{M}\sim r^{\eta}$ within $r_{\rm cool}$ – the radius at which the cooling time equals a Hubble time – with $\eta\approx 1$–1.5. A more comprehensive survey by Arnaud is summarized in Fig. 1. He plots the ratio of mass deposition within $r_{\rm cool}$, $\dot{M}_{\rm c}$, to that in the inner bin, $\dot{M}_0$, versus the ratio of the corresponding radii, $r_{\rm cool}/r_0$. For a power-law mass deposition profile this should give η. In practice, the point spread function of the IPC will tend to reduce $\dot{M}_0$ and so η will be overestimated, although the use of an incorrect gravitational potential can lead to an overestimate of $\dot{M}_0$ and so work the other way. It can be seen from this diagram that there are few clusters with $\eta>2$. The best-fit value is 1.2 and much of the scatter may be within the errors.

The most important conclusion from these results is that the ICM is not homogeneous on small scales but is in fact 'multiphase' consisting of 'blobs' at a range of densities. The method of analysis outlined above is strictly inconsistent since it assumes a single-phase medium. If, however, the density and temperature are regarded as characteristic of the gas dynamics then the results will not be too far off. A more detailed treatment is described in Section 1.2.

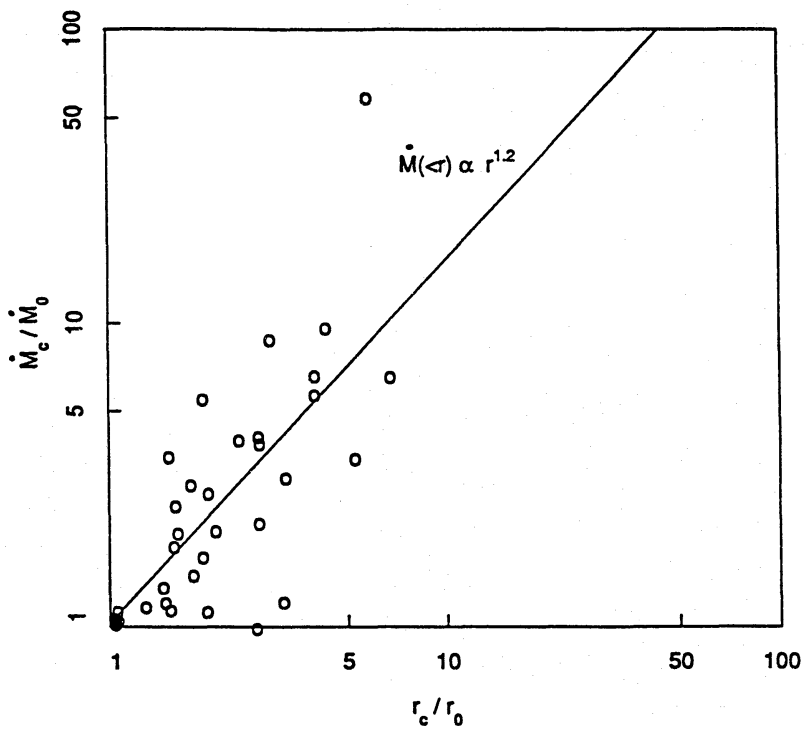

Figure 1. This figure shows the radial variation of the mass deposition profiles in clusters of galaxies. The ratio of the mass deposition rate within the cooling radius, $\dot{M}_{\rm c}$, to that in the central data-bin, $\dot{M}_0$, is plotted against the ratio of the cooling radius, $r_{\rm c}$, to the outer radius of the central bin, r_0. The circles represent the known cooling flow clusters (without error bars). This figure was supplied by Dr Arnaud.

The earliest theoretical models for the gas flow (e.g. Cowie & Binney 1977; Fabian & Nulsen 1977; Mathews & Bregman 1978) all assumed a homogeneous medium and therefore a constant mass inflow rate (for a steady state). More recently Thomas (1986) and White & Sarazin (1987a, b, c) have allowed for mass deposition, but at a rate which must be specified in a rather *ad hoc* manner.

1.2 MULTIPHASE FLOWS

What can we hope to gain from multiphase studies? First, to confirm the single-phase results. The homogeneous approximation is probably adequate to cope with the dynamics of the gas but not to follow the thermal evolution of gas blobs at a range of densities. Secondly, it is the structure of the density variation which determines the spatial distribution of the deposited matter. This is important if we are to understand the form of the observed mass deposition profiles or to examine the role of cooling flows in the context of galaxy formation; it is these points which are addressed most closely below. Finally, a knowledge of the size and structure of the individual cooling blobs is necessary to explain the form of the observed stellar initial mass function (Sarazin & O'Connell 1983; Johnstone, Fabian & Nulsen 1987) and to investigate the clustering of the products (e.g. the globular cluster hypothesis of Fall & Rees 1985). This aspect is not covered by the techniques described here.

When analysing such a flow, it is convenient to think of the system as having one spatial dimension (spherical symmetry) and one density dimension. This ignores the structure of the individual blobs, assuming only that their size is much smaller than that of the system as a whole. I should emphasize that the density perturbations required to cause deposition of gas at large radii lie in the non-linear regime. There has been much discussion about the rate of growth (or lack of it) of small, linear perturbations (Cowie, Fabian & Nulsen 1980; Nulsen 1986; Malagoli, Rosner & Bodo 1987; White & Sarazin 1987a; Balbus 1988); these would anyway be insufficient for the purpose.

Various assumptions are necessary in order to make progress. Fortunately there are physical reasons, first outlined by Nulsen (1986, hereafter N86) for a certain degree of simplification.

(i) The sound crossing time for density perturbations up to 1 kpc in size is so short that they will remain in pressure equilibrium until they cool to below 10^6 K.

(ii) In general one might expect that the different buoyancies of the various blobs would cause them to have different dynamics so that the physics of the interactions between them must be considered in solving the flow equations; in fact this is not necessary. N86 considered the forces acting on density perturbations and concluded that relative motions will tend to disrupt gas blobs and reduce their length scales so that their terminal velocities are small. Magnetic fields also help to pin blobs to the mean flow. Strictly speaking, this analysis only applies to a single overdensity in an otherwise uniform fluid and not to an emulsion of density phases. However, it is probably a good approximation to think of each blob as 'seeing' a background flow defined by all the other phases, since it turns out that most of the volume is occupied by a small range of densities. We make the simplifying assumption, without which further analysis is complicated considerably, that the density phases comove as they flow inwards.

(iii) Finally, it is assumed that the state of the flow is determined by initial conditions – i.e. there are no source terms either of mass, momentum, energy or density variation. This is probably a good approximation in clusters but will not be for flows in individual galaxies. In steady-state flows the density distribution need only be specified at the outer boundary. An alternative approach would be continually to introduce density variations throughout the flow, for example as a result of galaxy stirring. Apart from being strongly model-dependent it would seem difficult to create large density variations in this way.

Under these assumptions Thomas, Fabian & Nulsen (1987, hereafter TFN) have developed a multiphase deprojection method for analysis of the X-ray data which employs as many density phases within each radial shell as there are shells within that radius. This makes maximal use of the data and allows a self-consistent model for the gas flow. The results are in close agreement with those obtained using the previous single-phase method. Unfortunately, as the counts are partitioned in density as well as spatial bins this method can only be applied to the high-quality data from the centre of bright clusters and even these data are not good enough to determine the shape of the density distribution. Apart from a small core, which may be due to the point response function of the IPC, all the mass deposition profiles increase approximately linearly with radius, in agreement with the results shown in Fig. 1.

With the above assumptions it is also possible to derive analytic expressions for the evolution of density variations as they flow inwards and the form of the resulting mass deposition profile (N86). These can be solved exactly for certain families of self-similar density distributions which take a particular form at high densities. The resulting values of η, the mass deposition index, vary widely between approximately 0.5 and 3 with little reason to suggest a particular value for the index of about 1, as is observed.

This paper presents a multiphase, Lagrangian code, described in Section 2, which can be used to confirm and extend the above results. Steady-state models are used in Section 3 to investigate the development of density distributions as they flow inwards and the form of the resulting mass deposition profiles. Possible reasons are suggested for the similarity in observed mass deposition profiles. In Section 4 the dynamics of a family of self-gravitating, multiphase gas clouds are investigated. Preliminary results show that cooling flows may be important in the formation of giant elliptical galaxies. The results are summarized briefly in Section 5.

2 Description of the method

2.1 SINGLE-PHASE

The numerical method, outlined in Fig. 2, is based upon a conservative, Lagrangian scheme similar to that of Richtmyer & Morton (1957). It is spherically symmetric, consisting of $n_{\rm cell}$ concentric shells each of which may be split into several phases of differing density. I will first describe the equations for the case of a single gas phase within each cell. The variables are radius, r, velocity, u, time, t, mass, m, pressure, p, number density, n and temperature/specific energy, T. The gravitational acceleration, g, the artificial pressure, q, and the cooling function, Λ, also enter as functions to be specified. The radius, velocity and gravity are evaluated at the cell boundaries and the other quantities at the centres of cells; the velocity and artificial pressure are evaluated half a timestep ahead of the other variables.

First the radius and density are updated, and the artificial pressure calculated:

$$r_i' = r_i + u_i \Delta t \tag{1}$$

$$n_i' = 3m_i/[4\pi\mu m_{\rm H}(r_i'^3 - r_{i-1}'^3)] \tag{2}$$

$$q_i = \begin{cases} 0 & n_i' - n_i \leqslant 0 \\ [2\mu m_{\rm H}/(n_i'+n_i)]\,[Q(n_i'-n_i)(r_i'-r_{i-1}')/\Delta t]^2 & n_i' - n_i > 0 \end{cases} \tag{3}$$

where $\mu m_{\rm H}$, the mass per particle, is taken to be 10^{-24} g. The first two equations are self-explanatory. q is non-zero only when the volume of the shell is decreasing. It is introduced in order to smooth the boundaries of shock waves and expresses itself as an additional pressure opposing the contraction, but not the expansion, of shells. It has been found by experiment that the normalization, Q, should be set to approximately 2 (Richtmyer & Morton 1957). q is not time-

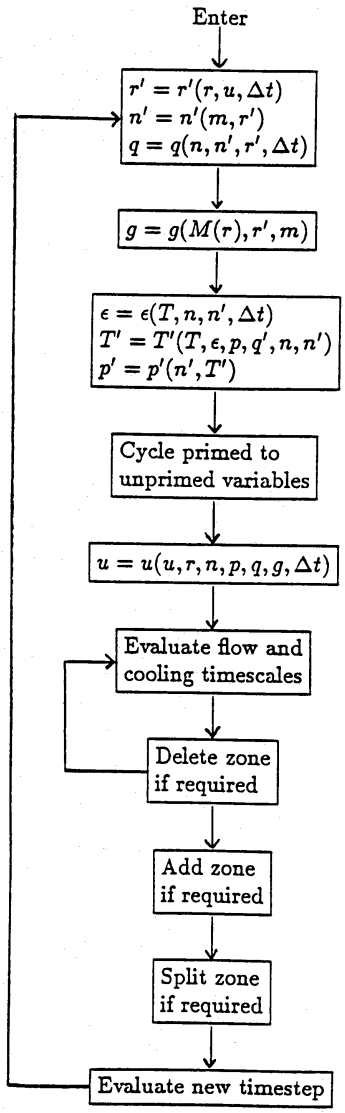

Figure 2. A flow diagram outlining the integration method.

centred in this scheme but, as it is somewhat arbitrary anyway, this does not matter. It is, however, implemented so as to conserve energy.

Next the gravitational acceleration is calculated:

$$g_i = \frac{GM(<r_i')}{r_i'^2}. \tag{4}$$

Here $M(<r)$ is the total mass within r:

$$M(<r_i') = M_{\rm gal}(<r_i') + \sum_{j=1}^{i} m_j. \tag{5}$$

The emissivity in units of 10^{-23} erg cm^{-3} s^{-1} is given by

$$n^2\Lambda = n_{\rm e} n_{\rm H} \begin{cases} 1.5\times10^{-3}T^{0.40} & 2\times10^7 < T \\ 9.0\times10^{5}T^{-0.80} & 1\times10^7 < T \leqslant 2\times10^7 \\ 2.5\times10^{-2}T^{0.28} & 4\times10^6 < T \leqslant 1\times10^7 \\ 3.0\times10^{5}T^{-0.79} & 1\times10^5 < T \leqslant 4\times10^6 \\ 0 & T \leqslant 1\times10^5 \end{cases} \tag{6}$$

where $n_e n_H = 0.229 n^2$. This is an analytic fit to the results of the optically thin emission code of Raymond & Smith (1977) for a 0.4 solar metallicity gas.

The temperature drop due to radiation, ε (which is proportional to the specific emissivity), and the new temperatures and pressures can now be evaluated:

$$\varepsilon_i = \frac{(n_i' + n_i)}{3k} \Lambda(T_i)\, \Delta t \tag{7}$$

$$T_i' = \left[3(T_i - \varepsilon_i) - \frac{(p_i + 2q_i)}{k} \left(\frac{1}{n_i'} - \frac{1}{n_i} \right) \right] \Big/ \left(4 - \frac{n_i'}{n_i} \right) \tag{8}$$

$$p_i' = k n_i' T_i', \tag{9}$$

where k is the Boltzmann constant. ε_i is not time-centred with respect to T_i but this error is small since the timestep is chosen so that ΔT_i is small. The equation for T is time-centred in p but not in q.

Lastly, the old variables are cycled to the new ($r_i = r_i'$ etc.) and then the velocities are updated.

$$u_i = u_i - \frac{2(p_{i+1} + q_{i+1} - p_i - q_i)\, \Delta t}{\mu m_H [n_{i+1}(r_{i+1} - r_i) + n_i (r_i - r_{i-1})]} - g_i \Delta t. \tag{10}$$

The denominator here is chosen so as to make the force $(1/\varrho)\partial p/\partial r$ continuous at the boundary between cells. It differs appreciably from the usual $\frac{1}{2}(n_i + n_{i+1})(r_{i+1} - r_{i-1})$ when there is a large density jump. This is not the case for the inflow models but can be important in situations where there are strong shocks. For the boundary conditions I take $u = 0$ at $r = 0$, with a constant pressure, p_{out}, acting at the outer boundary $r = r_{n\,cell}$.

At this stage conduction can be included if required. This is simply a transfer of internal energy between cells according to some prescribed function of T and r. I will not consider conduction here; to do so it would be necessary to make additional assumptions about the scale-size of the cooling blobs and the magnitude and morphology of magnetic fields.

This completes the stepping forward of the flow equations. Next the number of cells is adjusted. Any gas which has cooled to a temperature below 10^5 K would very quickly cool still further to 10^4 K. It has already radiated most of its energy and occupies a small volume. I remove such zones from the flow and adiabatically expand the next zone out into the space provided. In most cases, and always once the system has settled into a steady state, it is the central cell which is removed. The outer velocity of the cell immediately interior to the removed one is taken to be unchanged. This is somewhat arbitrary but does not matter appreciably since the Mach number of the flow is small.

As the outer boundary moves in, new cells of pressure p_{out} and a fixed temperature, T_{out}, are added at the outside. These increase in width as they move inwards and spatial resolution is lost. In a gravity-dominated flow this can be overcome by subdividing the cells as they pass within certain radii. In the constant pressure case, however, this does not lead to an increase in resolution as there is no interaction between cells; the subcells in this case continue to act as one unit.

Finally, a new timestep is evaluated based on the Courant and cooling-time conditions:

$$\text{(i)}\ \Delta t < c_r \min_i \left(\frac{r_i - r_{i-1}}{|u_i - u_{i-1}| + \sqrt{5kT_i/(3\mu m_H)}} \right), \qquad \text{(ii)}\ \Delta t < c_T \min_i \left(\frac{3kT_i}{2n_i \Lambda(T_i)} \right). \tag{11}$$

Both c_r and c_T are required to be less than unity for numerical stability and energy conservation. I take $c_r = c_T = 0.2$.

I have checked the code against analytic models such as constant pressure inflow; a static, self-

gravitating, non-radiating gas cloud; isothermal inflow (gravitational heating balancing cooling). In constant pressure flows (i.e. those in which gravity is negligible; I take $M_{\rm gal}=0$) the energy flux through the system is conserved to better than one part in 10^4. With large pressure differences between cells, however, energy is not conserved in the central bins where the errors in passing from differential equations describing smooth functions to difference equations evaluated at discrete points become large. For this reason the structure of the solution in the inner one or two bins should be treated with caution. The errors can be reduced by choosing a smaller bin size, or by subdividing cells as they flow into the centre. In the results presented below the errors are less than 1 per cent of the total energy flux through the system.

2.2 MULTIPHASE

In order to model a multiphase system, each radial shell, i, is split into several phases at a range of densities, $n_{j,i}$, $1\leqslant j\leqslant N_i$. The phases are forced to comove and are taken to be in pressure equilibrium. Taking n_i to stand now for the mean density within each shell, then the equations for velocity, radius, mean density, gravity and artificial pressure remain the same. Let $m_{j,i}$, $T_{j,i}$ and $\varepsilon_{j,i}$ stand for the appropriate quantities for each phase. Then we get the following equations (derived in the Appendix):

$$p_i'=\frac{3kn_in_i'/m_i\sum_{j=1}^{N_i}m_{j,i}(T_{j,i}-\varepsilon_{j,i})-(p_i+2q_i)(n_i-n_i')}{4n_i-n_i'} \tag{12}$$

$$\frac{1}{n_{j,i}'}=\frac{3k(T_{j,i}-\varepsilon_{j,i})+[(p_i'+p_i+2q_i)/n_{j,i}]}{4p_i'+p_i+2q_i} \tag{13}$$

$$T_{j,i}'=\frac{p_i'}{kn_{j,i}'}. \tag{14}$$

Note that in this case the $n_{j,i}'$ are not known beforehand and so ε can be time-centred in neither density nor temperature.

Phases are removed as they cool below 10^5 K, with those remaining being adiabatically expanded to occupy the extra volume. Since phases are removed from the cells, these become smaller in mass as they flow inwards. This reduces the problem of loss of spatial resolution in the centre. To test that the multiphase equations have been implemented correctly, I took several phases of equal density within each cell. These evolve exactly as in the case of a single phase at the same density. A further check is provided by the agreement with the analytic models of N86, described below.

3 Steady-state models

3.1 EVOLUTION OF DENSITY DISTRIBUTIONS

In this section I investigate the development of the density variations within the gas as it cools. I am only interested in the time-independent behaviour and so the system is allowed to run until a steady state is reached, with new cells being added at the outer radius to replace those which cool and are removed. The density distribution is described by the volume fraction, $f(\varrho, r)$, such that $f(\varrho, r)\,d\varrho$ is the fractional volume occupied by phases in the density range $[\varrho, \varrho+d\varrho]$. Each shell is given 50 phases, equally spaced in density, which are introduced at a mean temperature of 4.5×10^7 K and a pressure of 2.3×10^5 cm^{-3} K at 200 kpc. The density distributions used here are

Table 1. The models for the fraction volume distribution, $f(\varrho)$, of the density, discussed in the text. Model 1 is self-similar and is described by one parameter $\varrho_0(p)$. Models 2 and 3 have the same form as the asymptotic high-density 'cooling tail' described in the text. Models 4 and 5 are more steeply falling at high densities, and models 6 and 7 less so, than models 2 and 3. Finally, models 8 and 9 have a randomly generated, irregular distribution. Pictures of these distributions are shown in Fig. 3.

Model	$f(\rho)$	Range
1	$\rho^{-(4-\alpha)}\exp(-(\rho_o/\rho)^{(2-\alpha)})$	$\rho > 0$
2	$\rho^{-(4-\alpha)}$	$\frac{9}{10}\rho_h < \rho < \rho_h$
3	"	$\frac{1}{2}\rho_h < \rho < \rho_h$
4	$\rho_h - \rho$	$\frac{9}{10}\rho_h < \rho < \rho_h$
5	$\rho^{-(6-\alpha)}$	$\frac{1}{2}\rho_h < \rho < \rho_h$
6	$\rho - 0.89\rho_h$	$\frac{9}{10}\rho_h < \rho < \rho_h$
7	constant	$\frac{1}{2}\rho_h < \rho < \rho_h$
8	ragged	$\frac{9}{10}\rho_h < \rho < \rho_h$
9	"	$\frac{1}{2}\rho_h < \rho < \rho_h$

listed in Table 1 and sketched in Fig. 3. The simplest analytical example is model 1, $f(\varrho) \propto \varrho^{-(4-\alpha)} \exp[-(\varrho_0/\varrho)^{(2-\alpha)}]$, where α is the temperature dependence of the cooling function, $\Lambda \propto T^{\alpha}$. This distribution is unaltered by cooling in a constant pressure flow and the time evolution of model 1 using the code, shown in Fig. 4, clearly reproduces this behaviour accurately. Another simple example is the distribution of models 2 and 3, $f(\varrho) \propto \varrho^{(4-\alpha)}$, $\varrho_l < \varrho < \varrho_h$. Once again the shape is unaltered by cooling and in this case only the end points vary. The width of the distribution, $\Delta\varrho/\varrho$, merely determines how far the gas flows in before it begins to be deposited. Fig. 5 shows the evolution of this distribution in a constant pressure flow. α is 0.4 over the temperature range of interest, giving $f \propto \varrho^{-3.6}$. This form is maintained as the gas cools until it reaches temperatures where α is lower. The gravity-dominated case is similar.

The evolution of the shape of volume fraction distributions can be treated analytically under the assumption of a power-law cooling function and TFN derive the following expression for $f(\varrho, r)$:

$$f(\varrho, r) \propto \left(\frac{\varrho_R}{\varrho}\right)^{4-\alpha} f(\varrho_R; R), \tag{15}$$

where

$$\left(\frac{\varrho}{\varrho_R}\right) = \left[\left(\frac{p}{p_R}\right)^{(3/5)(2-\alpha)} + \left(\frac{\varrho}{\varrho_c}\right)^{2-\alpha}\right]^{1/(2-\alpha)}. \tag{16}$$

R denotes quantities evaluated at some reference radius – thus ϱ_R is the density at radius R of the phase with density ϱ at r, and $\varrho_c(r)$ is the 'critical density' – i.e. the density at R of the phase which reaches infinite density at r. This shows that all distributions develop a high-density tail of the form $f \sim \varrho^{-(4-\alpha)}$ as they cool. Broad distributions do not have time to alter their form, but sufficiently narrow initial distributions will become dominated by such a tail by the time matter

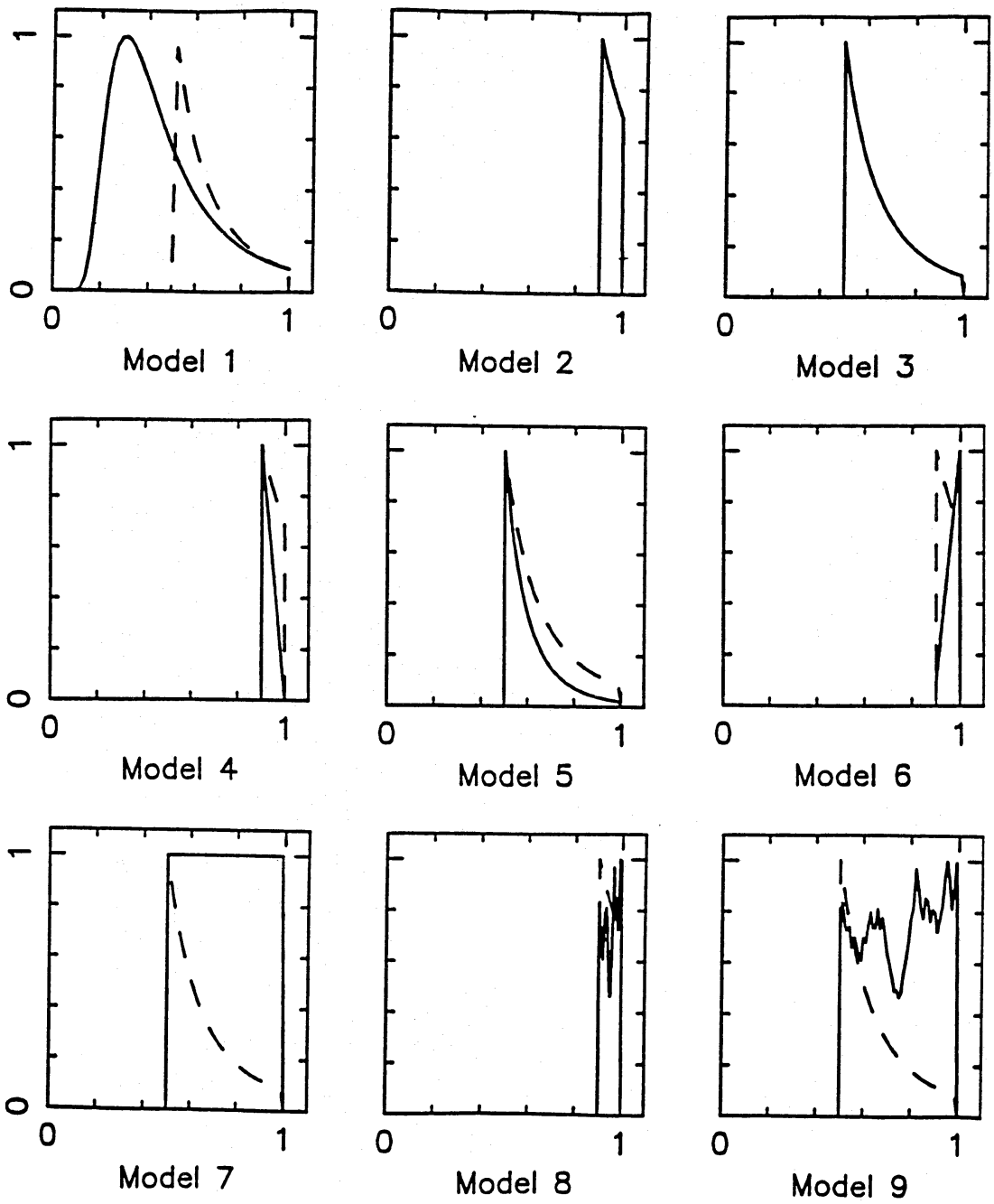

Figure 3. Pictures of the density distributions showing volume fraction plotted against density. In each case the coordinates have arbitrary normalization, although the position on the density axis is important. The dotted lines show $f \propto \varrho^{-(4-\alpha)}$ (model 2 or 3) plotted on the same scale.

begins to be deposited. This is illustrated in Fig. 5 which shows the evolution of a range of density distributions with $\Delta\varrho/\varrho=0.1$, models 2, 4, 6 and 8. The most discrepant case is model 6 which has a distribution that rises steeply to higher densities.

3.2 MASS DEPOSITION PROFILES

How does the form of the density variation relate to the spatial distribution of the deposited matter? I will concentrate on constant-pressure flows for which there are some analytic results. The simple models 1 and 2/3 have been integrated in N86. They give $\dot{M} \propto r^{\eta}$ with $\eta=3$ and $3(2-\alpha)/(5-2\alpha)$, respectively. These results are reproduced accurately by the code and are shown

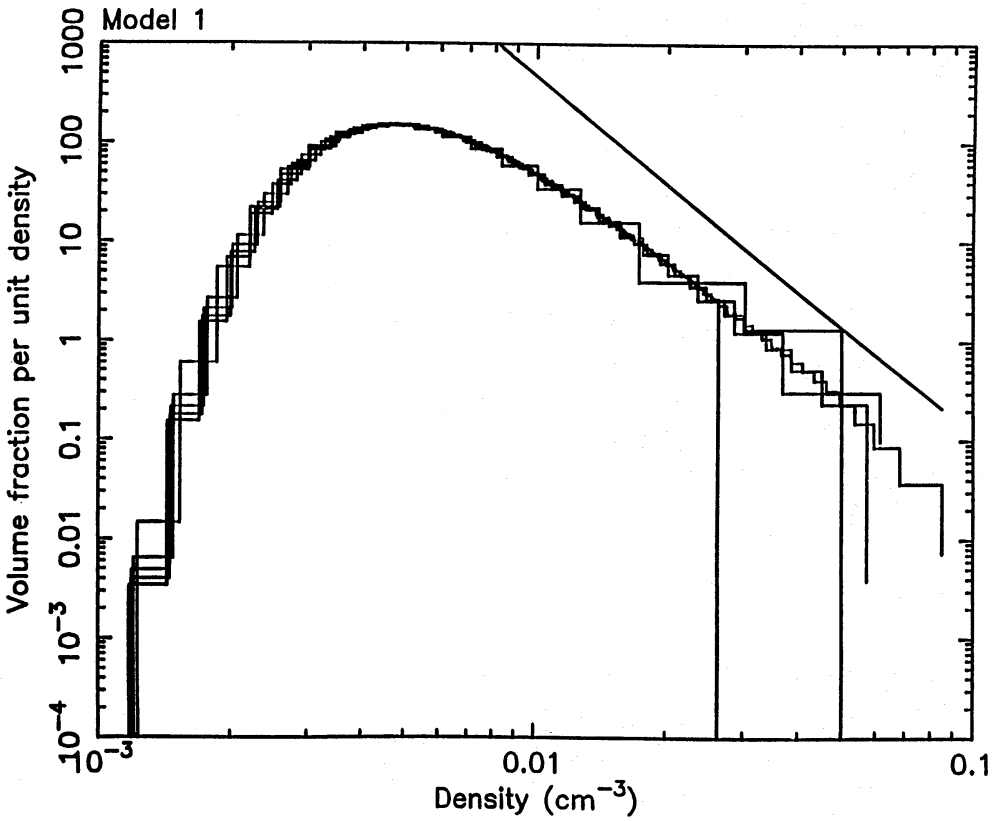

Figure 4. The time evolution of the density distribution of model 1 as it cools. Each of the five histograms shows the density distribution of the gas at a different stage in a constant pressure flow. As can be seen, they are identical except for a widening of the bin size. The straight line shows the asymptotic slope at high densities expected from cooling.

in Figs 6, 7 and 9. A formal fit to the mass deposition profile of model 2 gives $\eta \approx 1.36$ which is slightly larger than the theoretical index of 1.14 ($\alpha=0.4$) but gets closer to it as the resolution is increased, allowing more mass to drop out in the centre. A high resolution is not used in general as this increases the integration time of the runs.

It has been shown in the previous section that most initially narrow distributions differ only slightly from the form $f \sim \varrho^{-(4-\alpha)}$ by the time matter begins to be deposited. It is not surprising, therefore, that their mass deposition profiles, shown in Fig 7, resemble that of model 2. Once again the steeply rising example of model 6 is the most discrepant case with $\eta \approx 1.9$. These results are little changed by the inclusion of a massive halo in the gravitational potential in addition to that from the self-gravity of the gas. The largest inferred potentials correspond to masses of $\sim 10^{11} M_{\odot}\,\mathrm{kpc}^{-1}$, and the mass deposition profiles for models, 2, 4, 6 and 8 in this case are shown in Fig. 8. The effect of the halo is to pull the gas further in before it is deposited by the flow. This considerably alters the amount of mass reaching the central regions but does not much change the shape of the profile beyond this. Model 6, although it flows in further than the others, now gives a profile which is closer to $\dot{M} \sim r$ whilst the most discrepant case is now model 4 which falls steeply at high densities. Broad distributions do not have time to move towards the cooling distribution and so are deposited with a much wider range of profiles, Fig. 9. In this case, of course, the gas does not have to flow in so far before being deposited.

Paul Nulsen has suggested that his analytic models can be used to approximate a range of *narrow* density distributions. He considered a family of self-similar volume fraction distributions: $f \propto [1-(\varrho_m/\varrho)^{2-\alpha}]^{k-1}\varrho^{-(4-\alpha)}$, $\varrho > \varrho_m$. These all have the correct form at high density but grow as

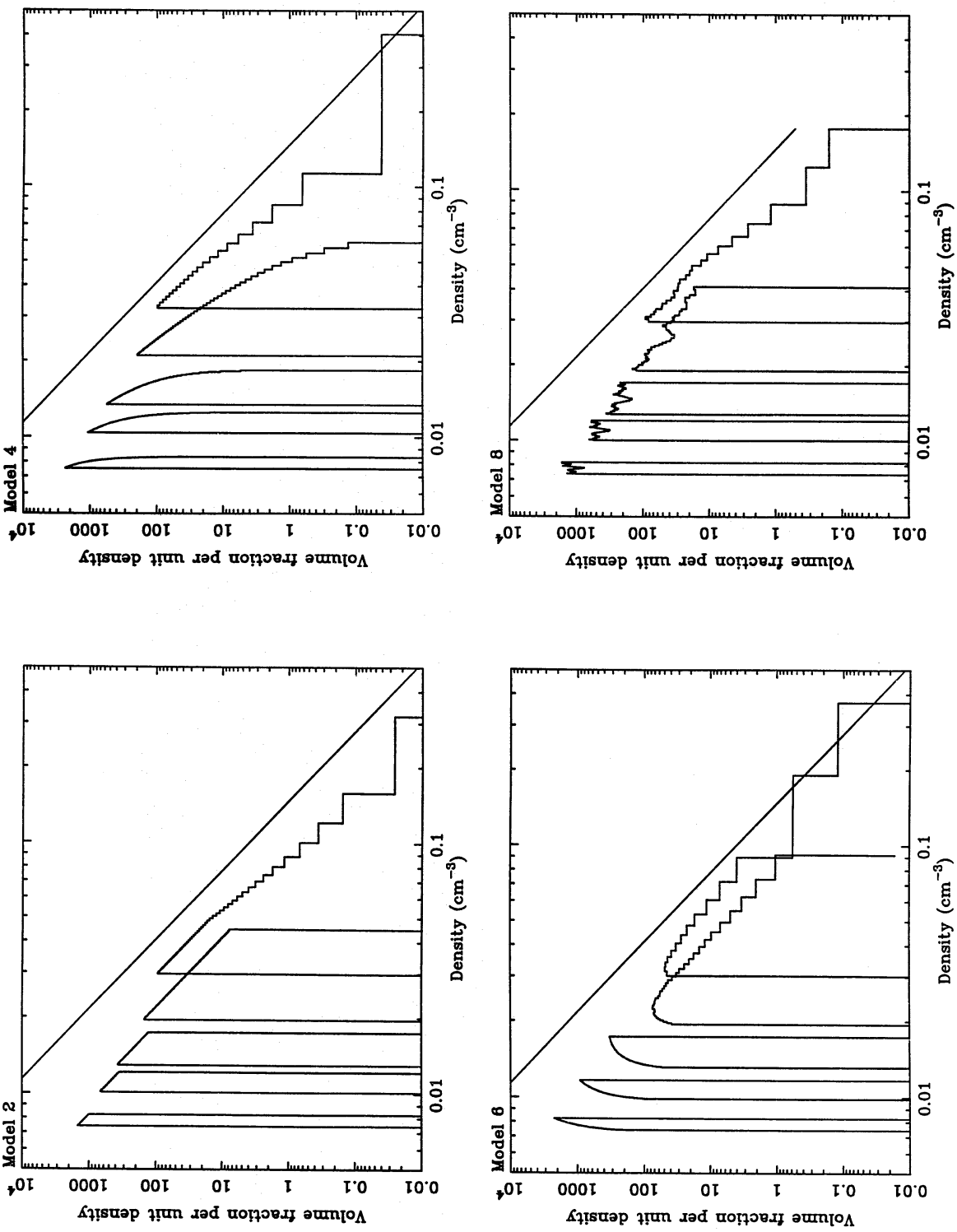

Figure 5. The time evolution of the density distributions of models 2, 4, 6 and 8 as they cool. Each of the five histograms shows the density distribution of the gas at a different stage in a constant pressure flow. The straight line shows the asymptotic slope expected from cooling. They each tend towards it except at high densities (i.e. corresponding to low temperatures) where there is a break to a different temperature dependence in the cooling function.

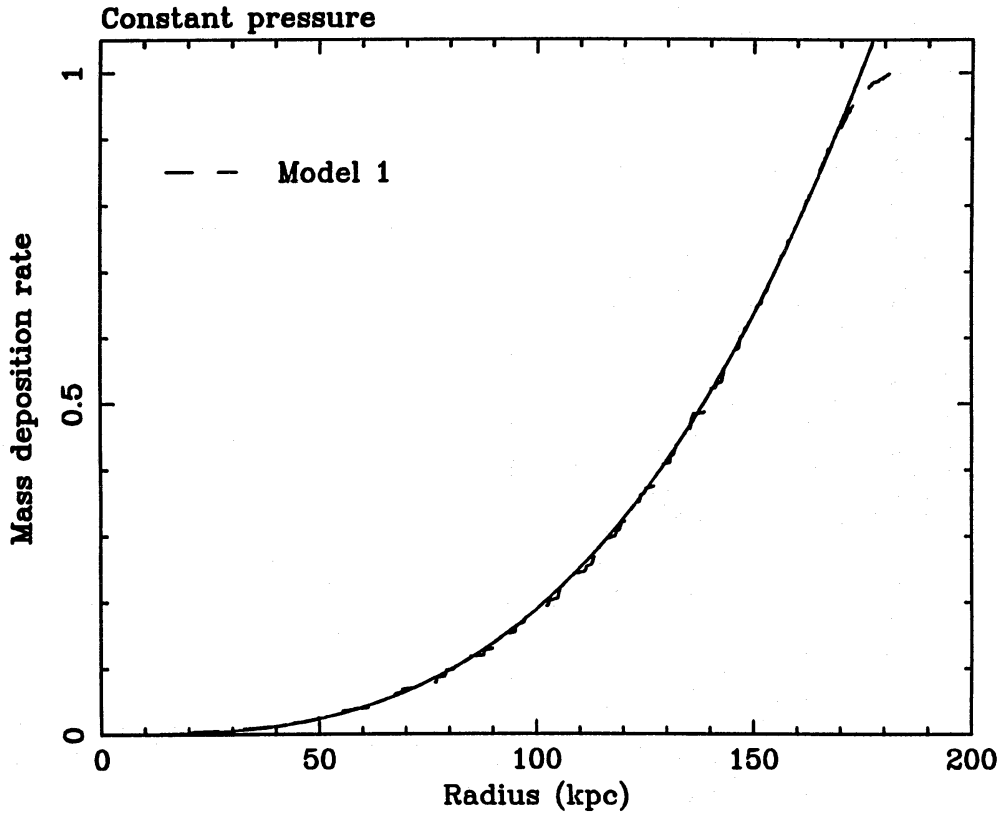

Figure 6. The dashed line shows the mass deposition profile, $\dot{M}(<r)$, for model 1 in a constant pressure flow and the solid line shows the thoretical profile, $\dot{M} \propto r^3$. The two are almost identical.

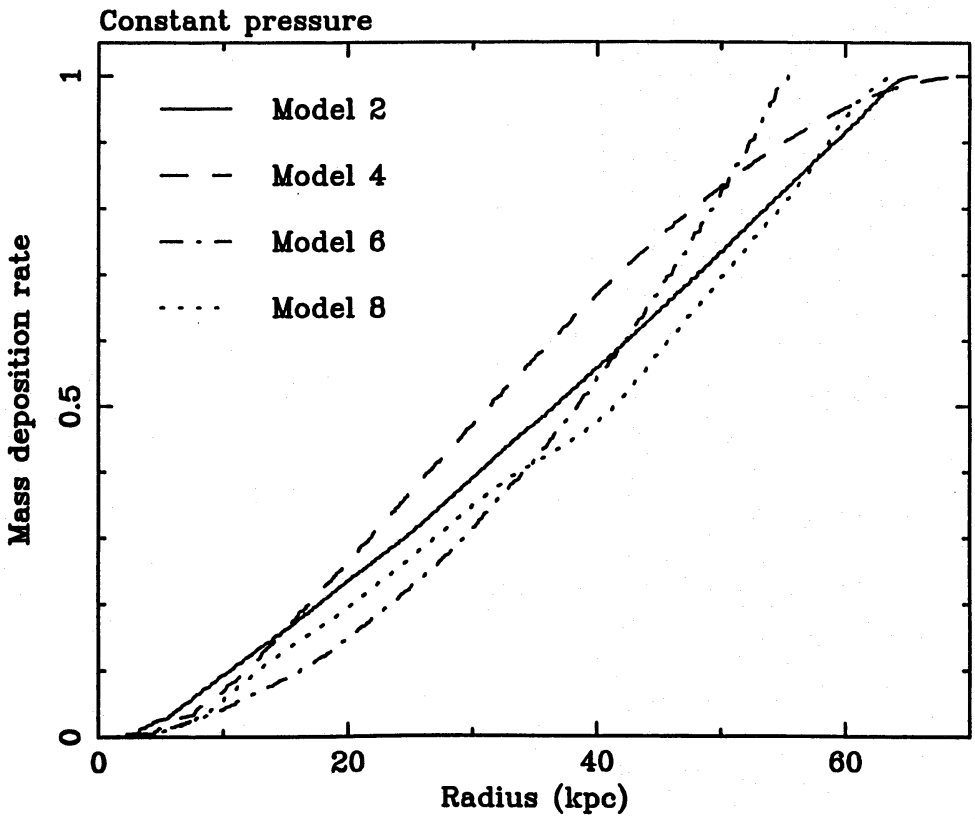

Figure 7. Mass deposition profiles, $\dot{M}(<r)$, for models 2, 4, 6 and 8 in a constant pressure flow. They all resemble $\dot{M} \sim r$, with model 6 being the most discrepant case.

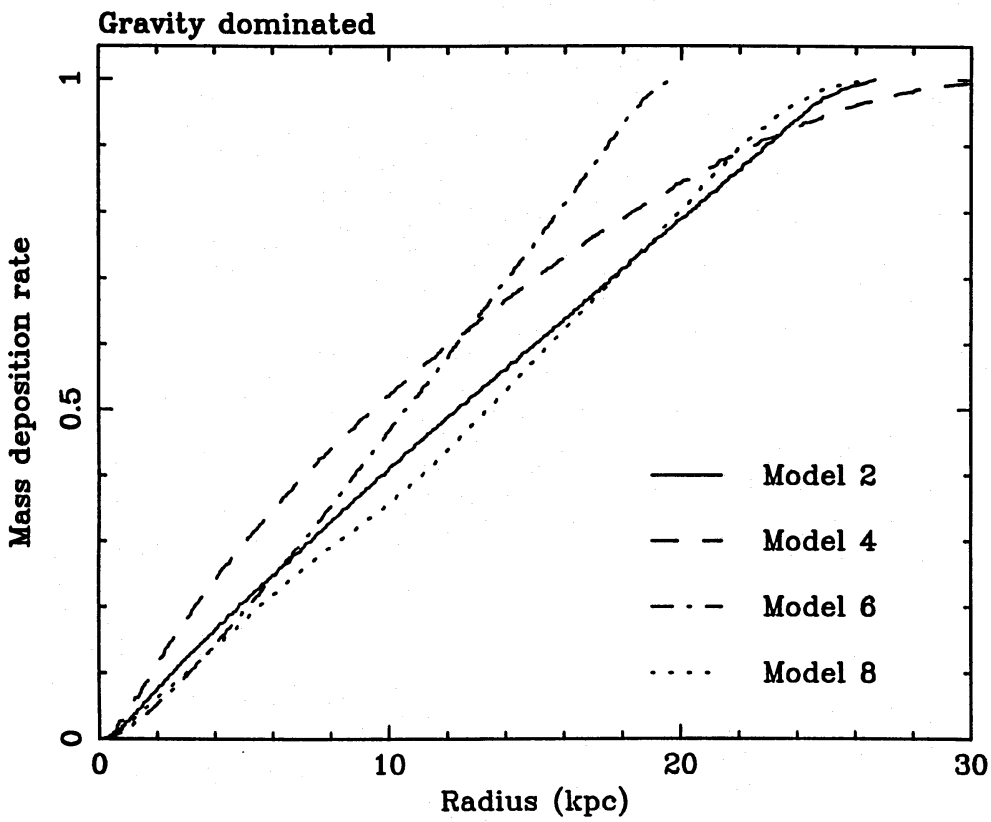

Figure 8. As for Fig. 7 but with the inclusion of a massive halo in the gravitational potential. The gas has been pulled further in and is deposited in a more centrally condensed manner. Model 4 now least resembles $\dot{M} \sim r$.

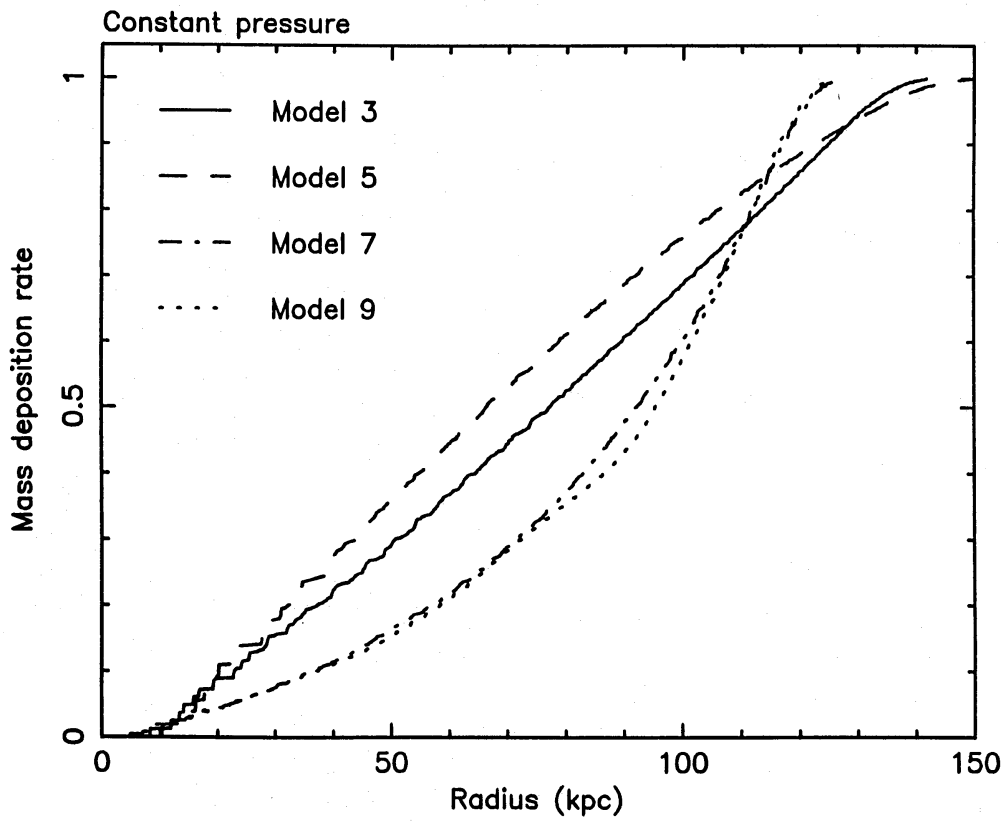

Figure 9. Mass deposition profiles for models 3, 5, 7 and 9 in a constant pressure flow.

power laws, $f \propto (\varrho - \varrho_m)^{k-1}$, near $\varrho = \varrho_m$. They have mass deposition profiles which are pure power laws with $\eta = 3(2-\alpha)k/[3-\alpha+(2-\alpha)k]$. If we consider a small portion of the distribution near $\varrho = \varrho_m$ then, due to self-similarity of the flow, this will behave in the same manner regardless of the distribution at high densities. Thus the mass deposition profile in the region where this gas is deposited will be a power law with the same η. With $\alpha = 0$ this gives $0.75 < \eta < 2$ for $-0.5 < (k-1) < 2$. Model 6 is similar to a $k=2$ distribution which has $\eta \approx 1.7$, in rough agreement with the value found above. More importantly, this analysis confirms the general trend shown in the above results, which can be summarized as follows: a density distribution resembling $f \propto \varrho^{-(4-\alpha)}$ will be deposited as $\dot{M} \propto r^{\eta}$ with η just larger than unity; those with $\varrho^{(4-\alpha)} f(\varrho)$ rising to high densities will be more extended, and those with $\varrho^{(4-\alpha)} f(\varrho)$ falling at high densities more centrally condensed, than this. In general, a Gaussian distribution, for example, might give a central core followed by a region in which $\dot{M} \sim r$ and then a smooth transition to constant $\dot{M}$ at large radii. If a density distribution is initially narrow then it will have longer to evolve towards $f \propto \varrho^{-(4-\alpha)}$ as it cools and so will give a mass deposition profile more closely resembling $\dot{M} \sim r$ than a broad distribution of the same shape.

3.3 ORIGIN OF THE DISTRIBUTION FUNCTION

The above discussion suggests that present-day X-ray observations of clusters are explained if the density distribution at any point resembles $f \propto \varrho^{-(4-\alpha)}$, and a detailed analysis of the development of narrow distributions suggests that a wide range of initial distributions might rise to this. Note that it is only necessary for the part of the distribution which corresponds to gas in the well-observed central regions of cooling flows to arise from a narrow distribution; there may be other high-density gas which is deposited at larger radii. However, only in the inner regions of observed cooling flows is the cooling time short enough for substantial evolution to have occurred. This would suggest that nearby cooling flows are the residuals of much larger flows in the past, a view which is reinforced by the time-dependent models considered in the next section. An alternative hypothesis is that the ICM is automatically created with broad density distributions of the correct form – at high densities cooling is dominant so that the asymptotic form of the cooling tail is almost assured.

The above discussion does not help to explain the sharp cut-off that the observations seem to require at low densities; for example, model 1 retains the same form no matter how long it is allowed to evolve and deposits matter as $\dot{M} \propto r^3$. One possibility is that the processes which act to tie density perturbations to the mean flow might be inefficient at preventing convection of low-density blobs; for example, overdense perturbations rapidly condense out of the flow once they become non-linear, whereas underdense perturbations remain. A relative motion which equals the inflow velocity is negligible when considering overdense perturbations, but is sufficient to decouple underdensities from the inflow. A more complete theory of multiphase media is needed to address this problem.

3.4 COMPARISON WITH CLUSTER OBSERVATIONS

It is important to verify that the code gives results in agreement with observations of cooling flows. The gas flow in a present epoch cluster is modelled by the following system. Gas is introduced at a radius of 500 kpc with a density of $10^{-3}\,\mathrm{cm}^{-3}$ and a temperature of 5×10^7 K. The range of densities is taken to be one-half the maximum density, with $f \propto \varrho^{-(4-\alpha)}$. Two alternative forms are used for the gravitational potential; both have a modified King law component, $M(<r) = (9\sigma^2/G)[1+(r/a)^2]^{-3/2}$, with $\sigma = 700\,\mathrm{km\,s}^{-1}$ and $a = 200$ kpc. In addition, one of the models, for which results are shown in Fig. 10, has a massive halo of the form

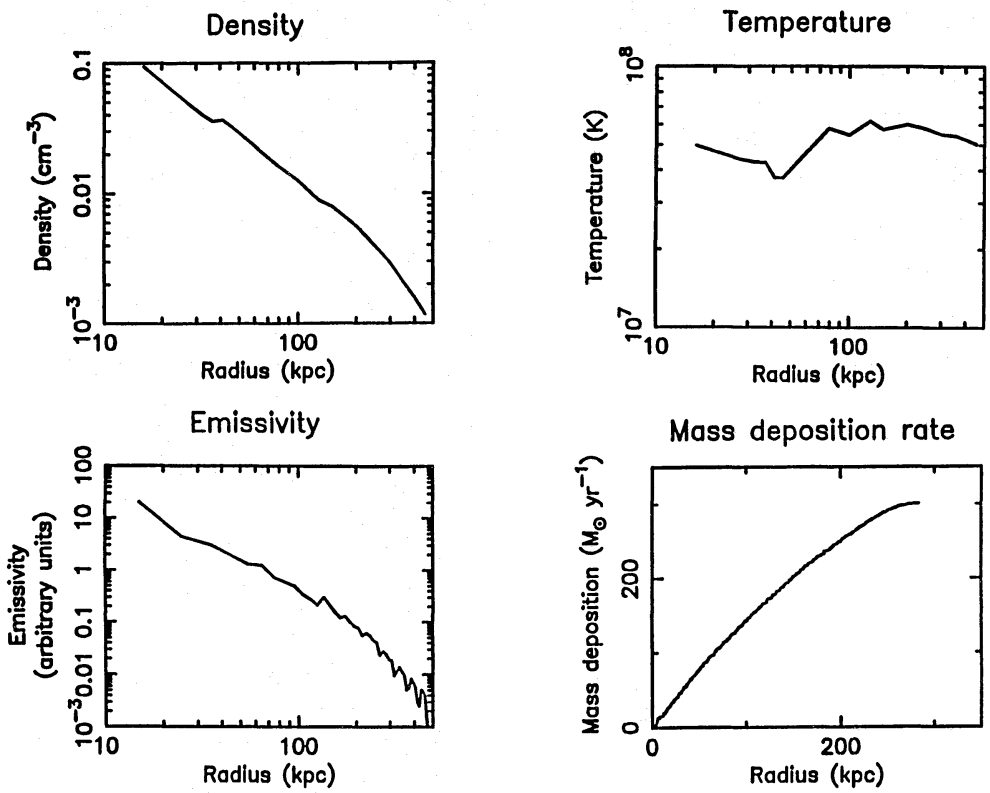

Figure 10. Results for a system resembling that of a present epoch cluster, with a massive halo in the gravitational potential.

$M(<r)=10^{11}(r/\mathrm{kpc})\,M_\odot$. In both cases the density falls as r^{-2} in the outer regions where the ratio of the virial to gas temperatures is $\beta=\sigma^2\mu m_\mathrm{H}/kT\approx 0.7$. This gives a pressure profile $p\sim r^{-2}$ and a surface brightness $\sim r^{-3}$, typical of the outer regions of many clusters. Within the core of the cluster potential the density profile flattens. Gravitational heating is reduced and so the temperature decreases as the gas flows inwards, though not as fast as for single-phase models. With no halo the gas density rises slightly less and the temperature decreases more towards the centre than shown in the figure. The count emissivity profiles are proportional to r^{-4} in the outer regions flattening to r^{-2} and $r^{-1.2}$ within the core for the halo and non-halo case, respectively. The mass deposition profiles are similar in form. With no halo the total flow rate is 250 $M_\odot$ yr^{-1} deposited uniformly in radius within 300 kpc; with one the gas is dragged further in giving 300 $M_\odot$ yr^{-1} within 270 kpc. These results compare with observations of cluster of galaxies. For instance, A 496 appears similar to the model which includes a halo. It has a count emissivity that rises as r^{-2} towards the centre and the volume fraction distribution is too peaked at low densities unless a massive halo is present. Some other clusters such as A 2199 have a flatter count emissivity profile in the centre. This suggests that gravity is less important, as in the non-halo case above, or that there is a core to the emission caused by a density distribution at low densities which is rising with density.

One feature which distinguishes multiphase from single-phase models is that the former have a large amount of gas cooling to low temperatures throughout the flow and not just in the centre. This leads to different predictions for the spatial variation of line strengths with radius. Fig. 11 shows for the inner region of (a) a single-phase flow and (b) a multiphase flow, the emission in various lines within shells of width 5 kpc. In the single-phase flow the low-energy lines are emitted only from the cool gas at the centre of the flow. There is, in effect, a range of radii for each line within which the gas has the required temperature. In the multiphase case, however, gas is cooling to low temperatures at all radii and so the line ratios remain almost constant throughout

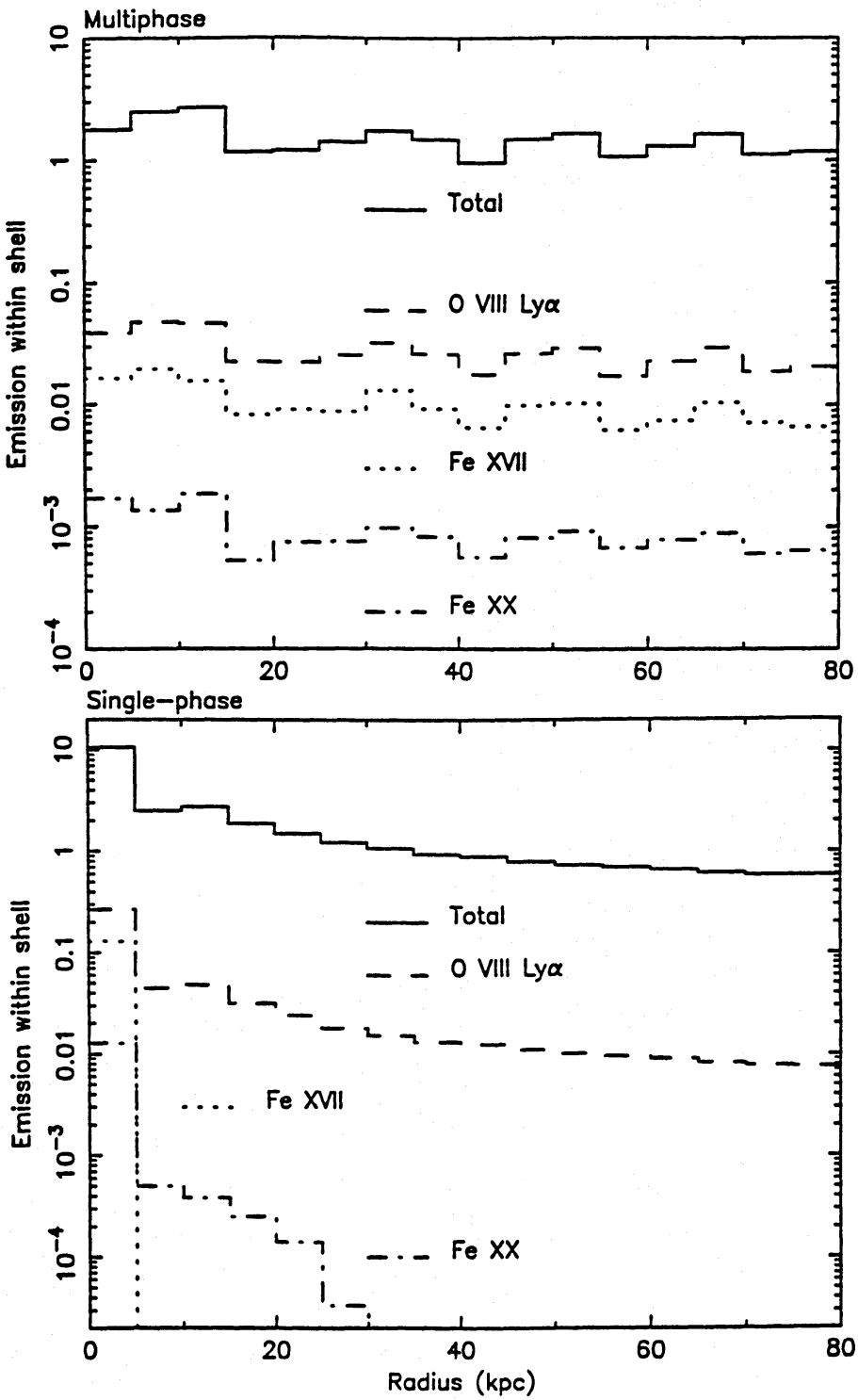

Figure 11. The total emission, and that from various lines, in shells of width 5 kpc. In the single-phase case the line emission is confined to the region of low temperature near the centre. In the multiphase case, however, gas is cooling through low temperatures throughout the flow and so the line ratios remain relatively constant.

the flow. Note also how the single-phase flow has a very much more centrally peaked luminosity profile, contrary to observations. This prediction of low-temperature lines at large radii will be an important future test of the models. A similar effect of varying hardness ratios for the X-ray emission has been noted by White & Sarazin (1987b).

It is not possible to model a galactic flow with mass and energy injection without making the model very dependent on the details of these processes. The observations are insufficient to constrain such models at the present.

4 Time-dependent models

4.1 INTRODUCTION

It has often been postulated that cooling flows may be important in certain types of galaxy formation. The rationale for this is the magnitude and form of the mass deposition profile. As mentioned in Section 1, the mass deposition rates in some clusters are as high as $500\,M_\odot\,\mathrm{yr}^{-1}$ giving total masses of more than $5\times10^{12}\,M_\odot$ in a Hubble time, which is comparable to the mass of the visible cd galaxy. In clusters of galaxies (Fig. 1; TFN) the mass deposition profiles follow $\dot{M}\sim r$ (with some scatter about this relation) and thus resemble those of the underlying mass distribution, although in the elliptical galaxy with the best X-ray data, NGC 4472, the mass deposition is more centrally condensed, i.e. more closely resembles the luminous galaxy (Thomas 1986). It is also interesting that the ratio of low- to high-mass star formation seen in nearby cooling flows is similar to the ratio of dark to luminous mass inferred from cluster dynamics (Fabian 1988). This suggests that cooling flows may process baryons to form both the luminous and dark components of galaxies; the cooling rates must then have been much larger in the past.

Clearly a time-dependent model is required with which to follow the evolution of cooling flows. Unfortunately this introduces many more free parameters into the system and until detailed, spatially resolved spectra become available observations of nearby flows pose little constraint. In this section I consider the collapse of primordial gas clouds to form elliptical galaxies. It is the general behaviour of models with a simple family of initial conditions which is of interest; a detailed discussion of individual models will be deferred to a later paper. Previously Silk (1977) and Rees & Ostriker (1977, hereafter RO) have investigated the effect of the ratio of the cooling and gravitational free-fall times on the evolution of homogeneous, primordial gas clouds after collapse and virialization in the early Universe. Masses of less than $\sim10^{12}\,M_\odot$ have cooling times which are short compared to the free-fall time and therefore form stars (or other condensed objects) *in situ* before collapsing dissipationlessly to form galaxies. In practice, of course, these clouds would not have time to virialize but would collapse directly into their final state. Larger masses (in the range 10^{12}–$10^{14}\,M_\odot$) initially have cooling times which exceed the free-fall time. These collapse in quasi-static equilibrium (with $n\propto T^3\propto r^{-3}$) until they reach a size of $\sim$75 kpc at which point the two time-scales become equal and they form a galaxy as above. Larger clouds ($\gtrsim10^{14}\,M_\odot$) have not yet had time to contract to 75 kpc. The mass range of large elliptical and central cluster galaxies is thus singled out as having this period of quasi-static collapse.

Here, a new element is introduced into this basic picture, that of local density variations in the gas clouds. Such inhomogeneities are expected to be present since the early Universe will contain density fluctuations on all scales which will be enhanced by, for example, the violent activity associated with metal enrichment of the gas. There is certainly evidence of large density variations throughout cooling flows in present day clusters. First the evolution of inhomogeneous clouds is investigated. The balance between cooling and inflow causes matter to be deposited over a large range of radii and can build massive haloes similar to those inferred to be present around giant elliptical galaxies. The implications of these results for galaxy formation including other aspects of more realistic cooling flow models are then discussed.

4.2 EVOLUTION OF GAS CLOUDS

In this section the evolution of pre-galactic, virialized gas clouds is investigated. There is no dark matter in the model except that which is provided by cooling of the gas. For simplicity, the gas is assumed to have been enriched to the currently observed metallicity by, for example, an early generation of Population III stars or mass ejection from the first small stellar systems; this process will also heat the gas. To make the clouds finite, and to eliminate boundary effects, an initially

polytropic equation of state is used, $p \propto \varrho^{\gamma} \propto T^{\gamma/(\gamma-1)}$, with $\gamma=\frac{5}{3}$. The clouds are taken to be spherically symmetric and are set up in hydrostatic equilibrium with zero outer pressure. The cloud mass, $M_{12}\times10^{12}\,M_{\odot}$, central number density, $n\,\mathrm{cm}^{-3}$, and a central temperature, $T_7\times10^7\,\mathrm{K}$, are then related by (Chandrasekhar 1939)

$$M_{12}\approx4.5n^{-1/2}T_7^{3/2} \tag{17}$$

and the outer radius, R kpc, is

$$R\approx17M_{12}T_7^{-1}. \tag{18}$$

For overdense perturbations in the early universe which have recollapsed and virialized by a time t_{vir} we have the following relation:

$$t_{\mathrm{vir}}\approx3.7\times10^8n^{-1/2}\ \mathrm{yr}, \tag{19}$$

which is an upper limit on the time if some reheating has taken place.

The gravitational free-fall time of a uniform gas cloud is

$$t_{\mathrm{grav}}=(3\pi/32G\varrho)^{1/2}\approx7\times10^7n^{-1/2}\ \mathrm{yr}. \tag{20}$$

More generally in the presence of a background gravitational potential I will take $t_{\mathrm{grav}}\sim\sqrt{2r^3/GM}$, where $M(r)$ is the mass within radius r. The constant-pressure cooling time, obtained by integrating the cooling function given in equation (6), is

$$t_{\mathrm{cool}}=n^{-1}C(T_7)\ \mathrm{yr}, \tag{21}$$

where

$$C(T_7)\approx T_7^{-1}\begin{cases}1.9\times10^7T_7^{2.79} & 1\times10^5<T\leqslant4\times10^6\\ -1.0\times10^6+1.2\times10^7T_7^{1.72} & 4\times10^6<T\leqslant1\times10^7\\ 3.7\times10^6+7.5\times10^6T_7^{2.80} & 1\times10^7<T\leqslant2\times10^7\\ -3.9\times10^7+3.1\times10^7T_7^{1.60} & 2\times10^7<T.\end{cases} \tag{22}$$

$C(T_7)$ is plotted in Fig. 12. The power-law approximation, $t_{\mathrm{cool}}\sim5kT/2(2-\alpha)n\Lambda$, holds over most of the range. The evolution of the clouds depends critically upon the ratio $\tau=t_{\mathrm{cool}}/t_{\mathrm{grav}}$ which is

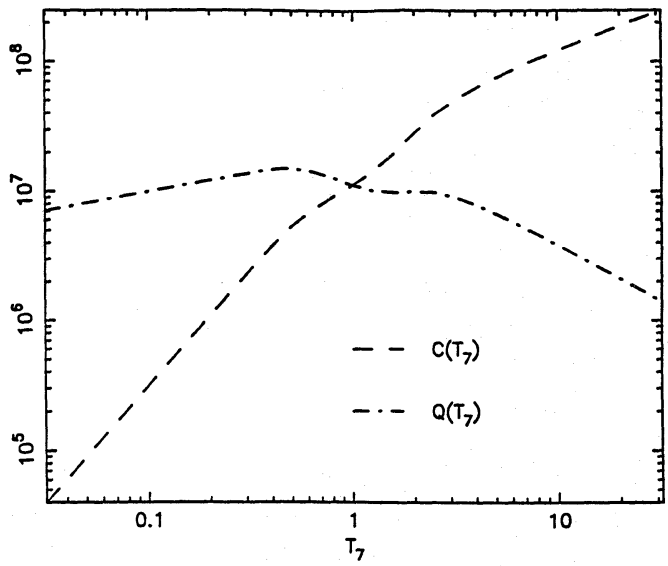

Figure 12. The cooling time per unit density, $C(T_7)$ yr, and the ratio of the cooling and free-fall times, $Q(T_7)$ – units as in equation (24), plotted as a function of the temperature, $T_7\times10^7\,\mathrm{K}$.

initially given by

$$\tau = t_{\rm cool}/t_{\rm grav} \approx \frac{n^{-1/2} C(T_7)}{7\times10^7}. \tag{23}$$

Using equation (17), this can be rewritten in terms of the mass of the cloud as

$$\tau = t_{\rm cool}/t_{\rm grav} \approx \frac{M_{12}}{3.2\times10^8}\, Q(T_7), \tag{24}$$

where $Q(T_7) = T_7^{-3/2} C(T_7)$ is also shown in Fig. 12. Note that Q has a maximum at $T_7 \approx 0.5$, hence $\tau \leqslant M_{12}/20$, and Q varies only by a factor of two over the range 3×10^6–3×10^7 K so that

$$\tau \sim \frac{M_{12}}{30}, \tag{25}$$

roughly independent of temperature. This means that, although the radius and time will scale with temperature, the form of the solution will be relatively independent of it. The mass scale given by equation (25) differs from that of RO mainly because of the difference in metallicity. If the gas clouds have not been enriched then the cooling function can be approximated above 2×10^6 K (where it has a minimum) by $\Lambda \approx 0.18 T_7^{0.45}$. This gives a power law expression for the cooling time similar to equation (21) with $C(T_7) \approx 2.8\times10^7 T_7^{0.55}$. The ratio of the cooling to the free-fall time is then $\tau \approx M_{12}/10 T_7^{-0.95}$ with a minimum $\tau \approx M_{12}/2$ at a temperature of 2×10^6 K. The mass scales are thus reduced by about an order of magnitude.

In multiphase gas clouds $t_{\rm grav}$ is unchanged but there is a range of cooling times. The evolution of the cloud is therefore modified, although to a limited extent it is similar to that of a uniform cloud at the same density. Models were chosen with a range of masses, to span the possible values of τ, and with a variety of density distributions.

The numerical method is altered slightly from the steady state described in Section 3. The deposited mass is stored in an Eulerian grid which represents the growing galaxy or cluster; it is assumed that the mass is deposited uniformly within each cell and does not move thereafter – i.e. it spends most of its time at the radius where it is deposited. In regions where the cooling time is shorter than, or comparable to, the gravitational free-fall time, it is no longer a good approximation to assume that when a zone is removed the next one out will adiabatically expand to take its place. In such situations each zone is divided into 30 new phases whenever the number of phases it contains drops to four. As the models are of self-gravitating clouds, additional zones do not have to be added at the outside during the integration. The initial configuration in each case contains 24 radial and 30 density bins.

The results are best interpreted with the aid of Fig. 13 which shows the range of possible values of $\tau = t_{\rm cool}/t_{\rm grav}$ (for the mean density) along the x-axis and the width of the density distribution, $\Delta\varrho/\varrho_{\rm max}$, along the y-axis. The evolution of the gas clouds splits the diagram into three regions, although the boundaries between these are not sharp and the properties vary continuously from one to the next.

In region A the cooling time of all the gas is less than $t_{\rm grav}$ and so most of it is deposited *in situ*. The opposite is true in region C where the cooling time of all the gas is initially long. Here the gas cloud undergoes a period of quasi-static contraction during which the mean density and temperature increase (roughly as $T \propto n^{1/3} \propto r^{-1}$), as does the range of densities at each radius. Eventually the highest density gas begins to be deposited and the ensuing cooling flow transports gas into the centre of the system. Finally, in region B, the range of cooling times in the gas extends above and below $t_{\rm grav}$. Some high-density gas is deposited *in situ*, followed by a cooling flow without an intervening period of quasi-static contraction.

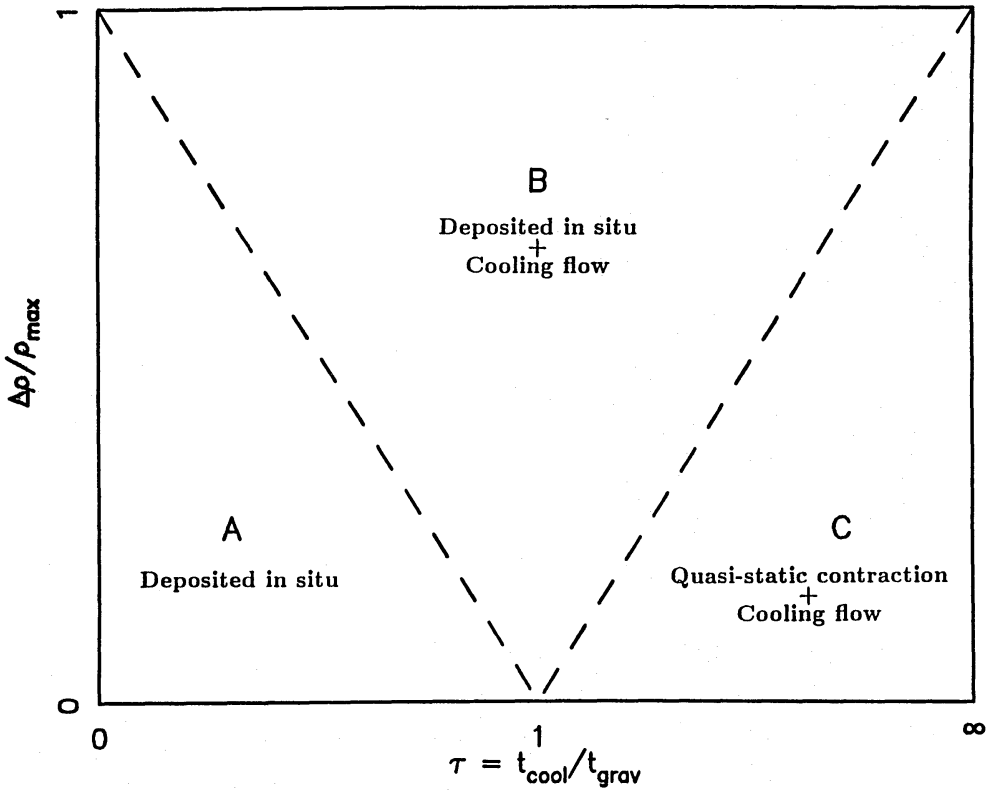

Figure 13. Behaviour of gas clouds with respect to position in the $\tau - \Delta\varrho/\varrho_{max}$ plane, as described in the text.

Individual clouds, as they evolve, move up and to the left on the diagram. Given time they will eventually reach the upper boundary and mass will begin to be deposited. (This is true only for the cores; gas in the outer regions may be depleted by inflow into the core.) The further to the right the clouds are on the diagram, the more important are the effects of inflow.

The diagram does not show the evolution of gas clouds at late times. Once a cooling flow is established it tends to evolve with a slowly decreasing core radius and increasing central density; this effect is more pronounced for flows with a larger value of τ. The degree of central concentration in the deposited density profile is dependent upon the form of the initial density distribution. Distributions with a greater amount of high-density gas tend to deposit gas at larger radii and hence give deposition profiles which are less peaked.

4.3 GALAXY FORMATION

What do the results tell us about the role of cooling flows in galaxy formation?

On the smallest mass-scales, for which $t_{cool} \ll t_{grav}$, there is no time to initiate a cooling flow and most of the gas cools *in situ*. In fact the gas clouds will not virialize in the first place and the models discussed above do not apply. There are several possible scenarios.

The gas may form stars (or other condensed objects) before collapsing dissipationlessly. The potential changes on a dynamical time-scale and so the system undergoes violent relaxation (Lynden-Bell 1967), driving it to final state which is relatively independent of the starting conditions. N-body simulations of this process have been carried out by, for example, Gott (1973, 1975), Aarseth & Binney (1978) and van Albada (1982). With the addition of 'cosmological infall', or with clumpy initial conditions, it is possible to produce models which resemble elliptical galaxies. There are some problems with this method, however. The dissipationless collapse implies that the final radius of the galaxy is not much smaller than the initial radius of the collapsing gas cloud which then requires a high formation redshift ($z \gg 10$) to produce compact

elliptical galaxies. Also it is not possible to produce high-density cores and fast rotation in small ellipticals without invoking dissipational collapse.

Alternatively, the gas may condense into high-density clouds which, in subsequent collisions, dissipate and form stars. Models of this form were first suggested by Larson (1969, 1974, 1975) and have more recently been investigated by Carlberg (1984). They can reproduce the density profiles, metallicity gradients and rotational support of elliptical galaxies but at the expense of a somewhat *ad hoc* requirement on the precise form of the star formation rate. It is also not clear why such a system of high-density clouds should arise in the first place without forming directly into stars.

Whatever the fate of the cooling gas, its removal will decrease the density of the residual gas and increase its cooling time. Provided that there is a sufficient range of densities in the initial gas cloud then there will be some gas (a naïve estimate suggests a fraction $1/\tau$) which is unable to cool in a dynamical time and which will thus get dragged in and heated to the virial temperature during the galaxy formation process. If the residual gas is not further heated and expelled from the galaxy by, for instance, supernovae explosions, then it will dissipate and settle into the core of the galaxy. To study the evolution properly it would be necessary to follow the motion of both the gas and the deposited stellar population in detail during the collapse (as in Larson's models). Nevertheless, in a crude model with an initial gas–galaxy mass ratio of 1/10, each component distributed as a King law $n \propto [1+(r/a)^2]^{-1.5}$, the central mass density more than doubled during the subsequent evolution showing that the residual inflow can have an important effect on the structure of the core. Of course, stellar mass loss will add to the inflowing gas, and the injection of dust and metals may considerably alter the mode of star formation. As much as 1/10 of the mass of the galaxy may be recycled in this way (see the models of MacDonald & Bailey 1981, Kunze, Loose & York 1987 and Loewenstein & Mathews 1987).

It has been assumed above that the dark matter is produced from the cooling gas. White & Rees (1978) consider a picture in which galaxies form in pre-existing dark haloes of dissipationless matter which later disperse as hierarchical clustering proceeds. If the gas comprises a fraction, F, of the total mass (taken to be fixed in value) and has the same spatial distribution, then τ is simply increased by a factor $1/F$. Luminous masses of up to $M_{12}=20F^2$ (or lower for primordial metal abundance) have τ less than unity and so can form inside the massive haloes. Larger masses do not have time to cool before the dispersal of the halo and will form galaxies only in exceptional circumstances. In practice the above masses seem rather low (for 0.4 solar abundance and $1/F\approx10$, or for primordial abundance and $1/F\approx3$, the characteristic luminous mass is that of an L^* galaxy).

On larger mass-scales for which $\tau\gtrsim1$, significant dissipative infall occurs. Single-phase models are uninteresting. They have a single stage of mass deposition which either deposits the gas uniformly (as in the above low-mass models) or drags it into the centre of the galaxy. With a wide range of densities, however, there is a balance between cooling and inflow which allows mass deposition over an extended period and in a manner not characterized by a single radius (i.e. with a power-law profile). There is first some deposition of high-density gas *in situ* but this may only be a small fraction of the total mass and so significant relaxation will not occur. This is followed by a prolonged period of inflow with the central density increasing and the core radius decreasing at later times. The deposition of matter is thus extended at first but gradually becomes more centrally condensed. One example with $M_{12}=30$ and $f\propto\varrho^{-3.6}$, $\Delta\varrho/\varrho=0.9$, whose time development is shown in Fig. 14, builds an r^{-2} halo which is similar in magnitude to those we infer to be present around central cluster galaxies and in this particular model there is $\sim5\times10^{12}M_\odot$ of gas remaining which will flow into the inner regions and add to the central galaxy. Note that the timescale for the evolution is so short that we would not expect to see evidence of such activity in observations of nearby cooling flows; these are controlled by the flow of gas into the galaxy from

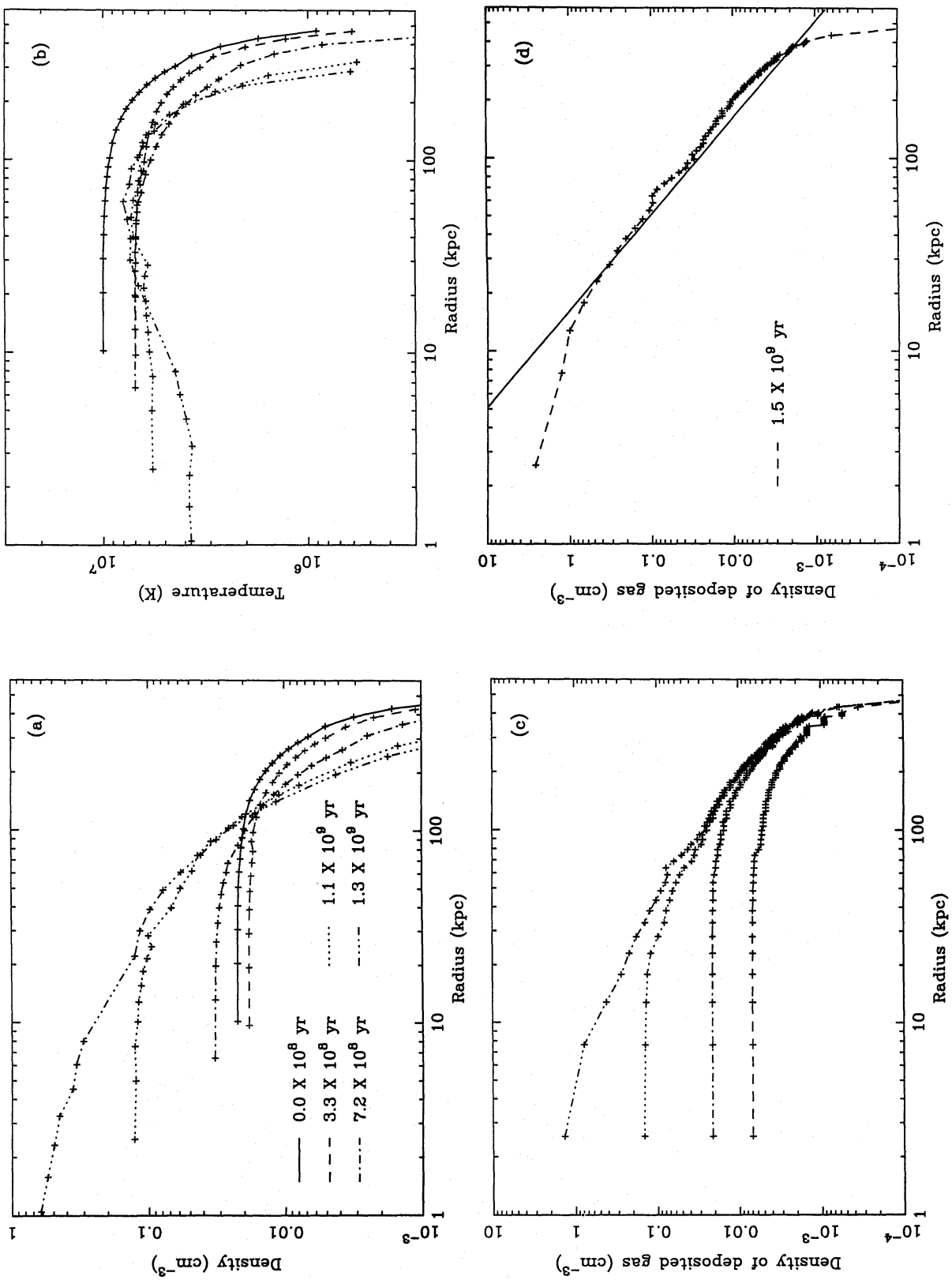

Figure 14. Plots of one particular collapsing gas cloud model at various stages in its evolution: (a) density of the gas, (b) temperature of the gas, (c) density of the deposited matter, (d) density of deposited matter after 1.5×10^9 yr (at which point spatial resolution is lost in the central regions) compared with a power law r^{-2}.

the surrounding ICM. The degree of central concentration of the dark matter depends upon the form of the density distribution; other models give profiles which are much more extended than this as there is more high-density gas. More work is necessary to examine the size of parameter space that gives rise to deposition profiles of the correct form and to investigate theoretically the expected form of the initial density distribution.

The degree of peaking is increased in larger flows for which there is a longer period of inflow. The largest mass scales, unless they initially contain a lot of high-density gas, eventually enter a stage of positive feedback between central gas density and mass deposition which results in a large fraction of their mass being deposited within a very small radius. Heating of the central gas and rotation or other departures from spherical symmetry may temper this process by maintaining a large core radius, and on the largest scales cooling flows may not yet have become established. However, in view of the fact that there are no observed cooling flows in which the mass deposition rates are currently high enough to form the central galaxy (although they are large enough to form the luminous component in some), the situation may be similar to that suggested by White & Rees (1978), discussed above. The high ratio of $t_{\rm cool}$ to $t_{\rm grav}$ means that dynamical evolution may prevent cooling flows from becoming established in cluster-sized systems. This agrees with observations: dynamically young systems with no single cd galaxy do not contain cooling flows (Jones & Forman 1984). Some high-density gas will have been deposited (indeed it forms the galaxies we see now) but each successive stage of clumping disrupts the central cooling flow.

It would be of interest to know the luminosity corresponding to the transition ($\tau\sim1$) between these modes of galaxy formation. Fabian *et al.* (1986) have derived a lower limit to the mass of early-type galaxies. When applied to a sample of bright galaxies this gives a mean mass-luminosity in excess of $70\,M_\odot/L_\odot$ and the true value may be many times this. The mass corresponding to L^* ($\approx5\times10^{10}\,L_\odot$) is then $M_{12}>3.5$. This mass gives a value of τ which is much less than unity for the models considered above. The actual value may be higher, however, since the mass estimate is a lower limit, and the metallicity may have been lower at the time of galaxy formation.

We thus see a transition in the mode of galaxy formation as τ increases through 1. For low values most of the gas has a short cooling time and only a small fraction of the mass is added at a later stage in a cooling flow. This fraction gradually increases, with τ, and the largest giant elliptical galaxies we see today at the centres of groups and clusters may be formed almost entirely by a cooling flow. On larger scales galaxy formation may be limited by the dynamical evolution of clusters.

4.4 CLUSTERS

To give the gas clouds a finite size and to remove the need for an outer boundary condition, the discussion has been limited to isolated systems. In reality each cloud will be embedded in some larger system and will accrete from it at later times; the cooling flows we see nearby are probably all of this type. It is the surrounding intracluster medium which provides the pressure normalization and thus determines the magnitude of the mass deposition. The cooling radii of observed systems lie within the halo of the central galaxy; within this radius the gas will once have been much denser and will therefore have evolved significantly. This is in accord with Section 3 which suggests an explanation for the similarity of the observed mass deposition profiles.

Low luminosity ellipticals have significant rotation and dissipational collapse models can account for this. At higher luminosities, however, angular momentum plays a less important role and velocity isotropies are more important in determining the shape of the galaxy. Cooling flow models are not necessarily in disagreement with this since turbulent viscosity can provide an effective mechanism for the removal of angular momentum. A small magnetic field reduces the effective mean free path of the gas particles to negligible values (this is the pretext for ignoring

conduction) so that the viscosity is small. The Reynolds number of the flow is then very large and we might expect turbulence to set in, even if the Rayleigh condition for instability (that the specific angular momentum decreases outward) is not satisfied (Landau & Lifschitz 1959). The specific energy dissipation rate in the turbulent motions will be of order $(\Delta u)^3/l$ where Δu is the velocity-scale and l the length-scale of the largest turbulent motions. This gives a time-scale for turbulent dissipation of $t_{\rm diss}\sim r/\Delta u\sim(r/v_{\rm flow})(v_{\rm flow}/\Delta u)$, so that during the time, $\sim r/v_{\rm flow}$, it takes for the gas to flow through the system the rotational velocities will be damped to be of the same order as the inflow velocity, which is very much less than the Keplerian velocity except, perhaps, within the core of the system.

It has been suggested by Toomre (1977) that elliptical galaxies form from mergers of spirals. However, this suffers from many problems (see Tremaine 1981 for a review). A more plausible hypothesis is that giant ellipticals in the centre of clusters may have formed by the merging of smaller ellipticals – the 'galactic cannibalism' hypothesis of Hausman & Ostriker (1978). Much of the circumstantial evidence for this process is explained, equally well, in the cooling flow model: the high luminosity of the central galaxy, the position at the cluster centre and the alignment of the major axis with that of the cluster. The observation that $\sim\frac{1}{4}$ of central galaxies have multiple nuclei (Hoessel 1980) is more direct evidence. However, many of these have high velocities relative to the central galaxy (Jenner 1974), and Tonry (1984) has suggested that they represent chance projections of galaxies on high-eccentricity orbits through the cluster centre. Merritt (1985) has questioned the high rates of merging predicted by other authors and suggests that cd galaxies form in subclusters at an early stage. The giant ellipticals found at the centres of poor groups are indeed found to be similar to those in richer clusters (Thuan & Romanishin 1981), although once again this can be interpreted in the cooling flow picture. One final piece of evidence, which is difficult to explain with the cannibalism hypothesis, is the higher globular cluster frequency of the brightest, central galaxies (see Hanes & Harris 1986).

The extensive haloes which are one of the defining characteristics of the cD galaxies in rich clusters (Oemler 1976) may either be high-density gas which has been deposited in the intracluster medium, or tidally stripped stars from cluster galaxies. They are unlikely to be associated directly with the formation of the central galaxy both because of their cluster-sized extent and the fact that they are not found around the central galaxies in poor groups.

Where do spirals fit into this picture? I have avoided discussing them so far both because they are not observed to have cooling flow activity (although, for example, the Sa/Sb Sombrero Galaxy, NGC 4594, has a deposition rate of $\sim\frac{1}{10}\,M_\odot\,{\rm yr}^{-1}$, Thomas *et al.* 1986) and because their structure does not fit into the standard spherically symmetric picture. One major difference between elliptical and spiral galaxies is the environment in which they are found and it seems probable that this is responsible for their different morphology. If both types of galaxy form from a cooling gas cloud then the initial collapse may form a halo and/or bulge in both cases. At later stages the absence of a high-pressure confining medium around spirals would prevent additional accretion and increase the cooling time relative to that in ellipticals. This, together with the freedom from galaxy interactions, may allow the gas to settle down into a disc.

5 Conclusions

The intracluster medium in clusters of galaxies which contain cooling flows is complex. Although single-phase models give a good description of the mean density, temperature and mass deposition within the flow they are unable to explain the observed mass deposition profiles or to follow the evolution of the system. For this reason a simple, source-free Lagrangian model has been developed to study the development of density distributions in the cooling gas. Initially narrow distributions tend towards a universal form as they cool which gives mass deposition profiles in

agreement with the observations. Time-dependent models of collapsing inhomogeneous gas clouds suggest that cooling flows play little part in the formation of low-mass galaxies (up to a few times $10^{12} M_{\odot}$) although infall at later stages can have an effect on the structure of the core. They can play an important role, however, in the formation of higher mass systems. The balance of cooling and inflow in a cooling flow can deposit matter in an extended r^{-2} profile resembling that of a massive halo.

In order to constrain the models it is important to know the density structure of the ICM. Little progress is likely to be made observationally until spatially resolved spectra become available with *ROSAT* and *AXAF*. A physical model for the formation of density variations in the ICM is not yet available but would be of great value.

The technique used above of introducing one density-dimension to describe the density variation, whilst it makes the models self-consistent, does not address the structure of individual blobs on small scales. This is a much harder problem about which little is known. The minimum blob size may be set by the scale on which conduction becomes effective or at which the blobs become tied to the mean flow; in either case magnetic fields will play a role. The point at which cooling gas goes out of pressure equilibrium and the value of the Jeans mass at the various stages will depend upon the pressure and metallicity. Ionizing radiation from the surrounding gas may also be important.

It is clear from the time-dependent models of Section 4 that the flows we observe today contain little information about past evolution; we are seeing the residual flow from the ICM on to the central galaxy. It is possible that a substantial fraction of the mass in galactic dark haloes may be processed through cooling flows and such a 'pervasive pre-galactic cooling flow' model has recently been examined by Ashman & Carr (1988). It is worth noting that the physical conditions in the gas at the time of galaxy formation were similar to those in current-day cooling flows regardless of whether or not the gas actually partook in a cooling flow.

The results on time-dependent cooling flow evolution presented here are only preliminary. Although the nature of the method restricts us to spherically symmetric studies, a more detailed analysis should be able to define the range of conditions over which the multiphase nature of the gas flow is important in models of galaxy formation.

Acknowledgments

I thank Keith Arnaud for supplying Fig. 1, Paul Nulsen and Andy Fabian for useful discussions, and the referee for making many suggestions which improved the clarity of the paper. This work was funded mainly by the SERC (UK) and in part by the NSERC. I am grateful for the hospitality of the IOA, Cambridge, where much of this work was carried out.

References

Aarseth, S. A. & Binney, J., 1978. *Mon. Not. R. astr. Soc.*, **185,** 227.
Arnaud, K. A., 1985. *PhD thesis,* Cambridge University.
Arnaud, K. A., 1988. Preprint.
Arnaud, K. A. & Fabian, A. C., 1988. Preprint.
Ashman, K. & Carr, B. J., 1988. *Mon. Not. R. astr. Soc.*, **234,** 219.
Balbus, S. A., 1988. *Astrophys. J.*, **328,** 395.
Carlberg, R. G., 1984. *Astrophys. J.*, **286,** 403.
Chandrasekhar, S., 1939. In: *An Introduction to the Study of Stellar Structure,* p. 96, Dover, New York.
Cowie, L. L. & Binney, J., 1977. *Astrophys. J.*, **215,** 723.
Cowie, L. L., Fabian, A. C. & Nulsen, P. E. J., 1980. *Mon. Not. R. astr. Soc.*, **191,** 399.
Fabian, A. C., 1988. In: *Proc. 1987 Rencontre de Moriond Meeting 'Starbursts and Star-forming Galaxies',* ed. Montmerle, T., Editions Frontières, in press.

Fabian, A. C., Hu, E. M., Cowie, L. L. & Grindlay, J., 1981. *Astrophys. J.*, **248,** 47.
Fabian, A. C. & Nulsen, P. E. J., 1977. *Mon. Not. R. astr. Soc.*, **180,** 479.
Fabian, A. C., Thomas, P. A., Fall, S. M. & White, R. E., 1986. *Mon. Not. R. astr. Soc.*, **221,** 1049.
Fall, S. M. & Rees, M. J., 1985. *Astrophys. J.*, **298,** 18.
Gott, J. R., III, 1973. *Astrophys. J.*, **186,** 481.
Gott, J. R., III, 1975. *Astrophys. J.*, **201,** 296.
Hanes, D. A. & Harris, W. E., 1986. *Astrophys. J.*, **309,** 564.
Hausman, M. A. & Ostriker, J. P., 1978. *Astrophys. J.*, **224,** 320.
Hoessel, J. G., 1980. *Astrophys. J.*, **241,** 493.
Jenner, D. C., 1974. *Astrophys. J.*, **191,** 55.
Johnstone, R. M., Fabian, A. C. & Nulsen, P. E. J., 1987. *Mon. Not. R. astr. Soc.*, **224,** 75.
Jones, C. & Forman, W., 1984. *Astrophys. J.*, **276,** 38.
Kunze, R., Loose, H.-H. & Yorke, H. W., 1987. *Astr. Astrophys.*, **182,** 1.
Landau, L. D. & Lifshitz, E. M., 1959. In: *Fluid Mechanics,* p. 116, Pergamon Press, Oxford.
Larson, R. B., 1969. *Mon. Not. R. astr. Soc.*, **145,** 405.
Larson, R. B., 1974. *Mon. Not. R. astr. Soc.*, **166,** 585.
Larson, R. B., 1975. *Mon. Not. R. astr. Soc.*, **173,** 671.
Loewenstein, M. & Mathews, W. G., 1987. *Astrophys. J.*, **319,** 614.
Lynden-Bell, D., 1967. *Mon. Not. R. astr. Soc.*, **136,** 101.
MacDonald, J. & Bailey, M. E., 1981. *Mon. Not. R. astr. Soc.*, **197,** 995.
Malagoli, A., Rosner, R. & Bodo, G., 1987. *Astrophys. J.*, **319,** 632.
Mathews, W. G. & Bregman, J. N., 1978. *Astrophys. J.*, **224,** 308.
Merritt, D., 1985. *Astrophys. J.*, **289,** 18.
Nulsen, P. E. J., 1986. *Mon. Not. R. astr. Soc.*, **221,** 377.
Oemler, A., Jr, 1976. *Astrophys. J.*, **209,** 693.
Raymond, J. C. & Smith, B. W., 1977. *Astrophys. J. Suppl.*, **35,** 419.
Rees, M. J. & Ostriker, J. P., 1977. *Astrophys. J.*, **179,** 541.
Richtmyer, R. D. & Morton, K. W., 1957. In: *Difference Methods for Initial Value Problems,* p. 318, Interscience, New York.
Sarazin, C. L., 1986. *Rev. mod. Phys.*, **58,** 1.
Sarazin, C. L. & O'Connell, R. W., 1983. *Astrophys. J.*, **268,** 552.
Silk, J., 1977. *Astrophys. J.*, **211,** 638.
Stewart, G. C., Canizares, C. R., Fabian, A. C. & Nulsen, P. E. J., 1984. *Astrophys. J.*, **278,** 536.
Thomas, P. A., 1986. *Mon. Not. R. astr. Soc.*, **220,** 949.
Thomas, P. A., Fabian, A. C., Arnaud, K. A., Forman, W. & Jones, C., 1986. *Mon. Not. R. astr. Soc.*, **222,** 655.
Thomas, P. A., Fabian, A. C. & Nulsen, P. E. J., 1987. *Mon. Not. R. astr. Soc.*, **228,** 973.
Thuan, T. X. & Romanishin W., 1981. *Astrophys. J.*, **248,** 439.
Tonry, J. L., 1984. *Astrophys. J.*, **279,** 13.
Toomre, A., 1977. In: *Evolution of Galaxies and Stellar Populations,* p. 401, eds Tinsley, B. M. & Larson, R. B., Yale University Press, New Haven.
Tremaine, S., 1981. In: *Structure and Evolution of Normal Galaxies,* p. 67, eds Fall, S. M. & Lynden-Bell, D., Cambridge University Press, Cambridge.
van Albada, T. S., 1982. *Mon. Not. R. astr. Soc.*, **201,** 939.
White, R. E., III & Sarazin, C. L., 1987a. *Astrophys. J.*, **318,** 612.
White, R. E., III & Sarazin, C. L., 1987b. *Astrophys. J.*, **318,** 621.
White, R. E., III & Sarazin, C. L., 1987c. *Astrophys. J.*, **318,** 629.
White, S. D. M. & Rees, M. J., *Mon. Not. R. astr. Soc.*, **183,** 341.

Appendix: Multiphase numerical equations

We wish to derive the analogous expressions to equations (7)–(9) of Section 2, for the multiphase case. First note that the radiative temperature drop is taken to be

$$\varepsilon_{j,i}=\frac{2n_{j,i}}{3k}\,\Lambda(T_{j,i})\,\Delta t, \tag{A1}$$

which is not time-centred in either density or temperature since neither of these are known in

advance. The error will be small provided these quantities do not change very much during one time-step. We then have

$$T'_{j,i}=T_{j,i}-\frac{2}{3k}\left(\frac{p_i+p'_i}{2}+q_i\right)\left(\frac{1}{n'_{j,i}}-\frac{1}{n_{j,i}}\right)-\varepsilon_{j,i} \tag{A2}$$

$$p'_i=kn'_{j,i}T'_{j,i}, \tag{A3}$$

for $1\leqslant j\leqslant N_i$, and

$$\sum_{j=1}^{N_i}\frac{m_{j,i}}{n'_{j,i}}=\frac{m_i}{n'_i}. \tag{A4}$$

These give $2N_i+1$ implicit equations for the $2N_i+1$ unknowns $T'_{j,i}$, $n'_{j,i}$ and p'_i. The $T'_{j,i}$ can be eliminated by substituting equations (A3) into (A2), giving, after rearrangement,

$$\frac{1}{n'_{j,i}}=\frac{3k(T_{j,i}-\varepsilon_{j,i})+[(p'_i+p_i+2q_i)/n_{j,i}]}{4p'_i+p_i+2q_i}. \tag{A5}$$

These can then be summed, as in equation (A4), to eliminate the $n'_{j,i}$:

$$\sum_{j=1}^{N_i}\frac{m_{j,i}}{n'_{j,i}}=\frac{3\sum m_{j,i}(T_{j,i}-\varepsilon_{j,i})+(p'_i+p_i+2q_i)\sum m_{j,i}/n_{j,i}}{4p'_i+p_i+2q_i}, \tag{A6}$$

which gives

$$p'_i=\left[\frac{3kn_in'_i}{m_i}\sum_{j=1}^{N_i}m_{j,i}(T_{j,i}-\varepsilon_{j,i})-(p_i+2q_i)(n_i-n'_i)\right]\Big/(4n_i-n'_i). \tag{A7}$$

This is exactly analogous to equation (8), which gives the new temperature (and hence pressure) for the single-phase case, but with uniform quantities being replaced by the appropriate means. Equations (A1), (A7), (A5) and (A3), taken in that order, then give explicit expressions for the new quantities.